1 # Transient Wind-driven Polynyas Within Nares Strait

2 **Kevin Joshy[1], G.W.K. Moore[1, 2], Kaitlin McNeil[1, 2]**

3 [1]Department of Chemical and Physical Sciences, University of Toronto, Mississauga,
4 Mississauga, Canada. [2]Department of Physics, University of Toronto, Toronto, Canada.

5 Corresponding author: G. W. K. Moore (gwk.moore@utoronto.ca)

6 **Key Points:**

7 - Previously unknown wind-driven polynyas form downwind of Joe and Franklin Islands
8   within Nares Strait during autumn months
9 - The presence of these islands interrupting the sea ice flow through the strait are proposed
10   to be the drivers inducing polynya formation
11 - The size and extent of these polynyas was correlated with wind speed flowing
12   southwards through the strait

13 **Abstract**

14   Nares Strait, situated between northwest Greenland and Ellesmere Island is a major sea

15 ice export path from the Arctic Ocean. One of the narrowest parts of the strait — Kennedy

16 Channel — is host to several islands. These obstacles' impact on the ice flow along the Strait has

17 yet to be investigated. Here we show that during autumn, these islands can interrupt the

18 relatively homogenous sea ice flow through Kennedy Channel, carried by wind and water

19 currents, and shield downstream regions from becoming ice-covered, resulting in the formation

20 of hitherto unknown transient polynyas, whose size and extent were correlated with the wind's

21 strength and direction along Kennedy Channel. These polynyas likely impact the regional

22 meteorology and oceanography through enhanced air-sea fluxes of heat, moisture, momentum,

23 and carbon dioxide. The presence of open water may also impact the complex and productive

24 regional ecosystem.

25 **Plain Language Summary**

26   Nares Strait is a passageway situated between Ellesmere Island — the northernmost

27 island of Nunavut, Canada — and Greenland. The southern end of this channel is the site of

28 formation of the North Water Polynya (NOW) which is an open water expanse that forms in the

29 midst of thick surrounding ice. Open water regions of polynyas throughout the world, in general,

30 have major impacts on local climates because they facilitate interactions from the atmosphere to

31 the sea and vice versa. The NOW in particular sustains a major Arctic ecosystem that nearby

32 human communities depend on for resources as well. We identify polynyas that form in the

33 interior of Nares Strait during autumn whose sizes are related to the strength of southward winds

34 blowing through the channel. These polynyas likely also impact the regional climate and ocean

35 dynamics, and may serve as a site of Arctic species habitation both in the present and in a future

36 where the integrity of the NOW is potentially compromised due to a changing Arctic

37 environment.

38 **1 Introduction**

39   Polynyas are defined as regions of open water found within a surrounding area of sea ice

40 and tend to form by two distinct mechanisms (Barber & Massom, 2007); those that form via the

41 melting of ice due to heat fluxes from processes such as the upwelling of warm waters are called

42 sensible heat polynyas (Smith et al., 1990), while those that form via the exposure of open water

43   by winds that drive away ice cover are referred to as latent heat or wind-driven polynyas (Barber

44   & Massom, 2007). Despite this classification, many polynyas around the world form as a result

45   of some combination of these two effects (Barber & Massom, 2007).

46   Polynyas are important meteorologically, oceanographically, and biologically. They

47   contribute to atmospheric forcing via significant sea-air heat and moisture fluxes (Kottmeier &

48   Engelbart, 1992), they influence ocean salinity via processes such as frazil ice formation and

49   brine rejection (Smith et al., 1990), as well as encouraging the formation of dense water

50   (Weingartner et al., 1998). Biologically, they allow for the upwelling and mixing of nutrient-rich

51   waters (Arrigo, 2007) which, in combination with enhanced solar insolation at the active polynya

52   site (Tremblay & Smith, 2007), encourage biological activity.

53   Nares Strait, a passageway situated between Ellesmere Island, the northernmost island of

54   Canada, and northwestern Greenland (Fig. 1) connects the Arctic Ocean at its north to the

55   subpolar North Atlantic at its south. Nares Strait is a significant site of sea ice export, which is

56   driven by wind and ocean currents, out of the Arctic Ocean and experiences an average seasonal

57   sea ice area flux on the order of 100×10^3 km² (Howell et al., 2023). This is approximately 10%

58   of the export through Fram Strait (Smedsrud et al., 2017).

59   The polynya that forms annually over northern Baffin Bay — the North Water Polynya

60   (NOW) — *Pikialasorsuaq* in Greenland (Moore et al., 2023) and *Sarvarjuaq* in Nunavut —

61   appears as a result of the cessation of sea ice flow through the strait due to the formation of an

62   ice arch near the strait's southern terminus (Barber et al., 2001; Ribeiro et al., 2021). The

63   inhibition of further sea ice flow by these arches, alongside the wind-forced advection of sea ice

64   out of the downstream region (Barber et al., 2001; Moore & Imrit, 2022), and the melting of ice

65   via the thermodynamic interaction with warm subsurface waters (Steffen, 1985) are together

66   suggested to maintain the integrity of the NOW (Ingram et al., 2002).

67   A large body of evidence suggests the presence of a vast ecosystem that the NOW

68   sustains. Phytoplankton blooms are common and promoted in polynyas (Marchese et al., 2017;

69   Tremblay & Smith, 2007), which act as a foundation for an Arctic food web. Several animal

70   populations have also been documented in this region such as beluga whales, narwhals, walruses,

71   bearded seals, seabirds, as well as limited sightings of polar bears, many of which overwinter in

72   the NOW (Finley & Renaud, 1980; Heide-Jørgensen et al., 2013, 2016; Møller et al., 2018;
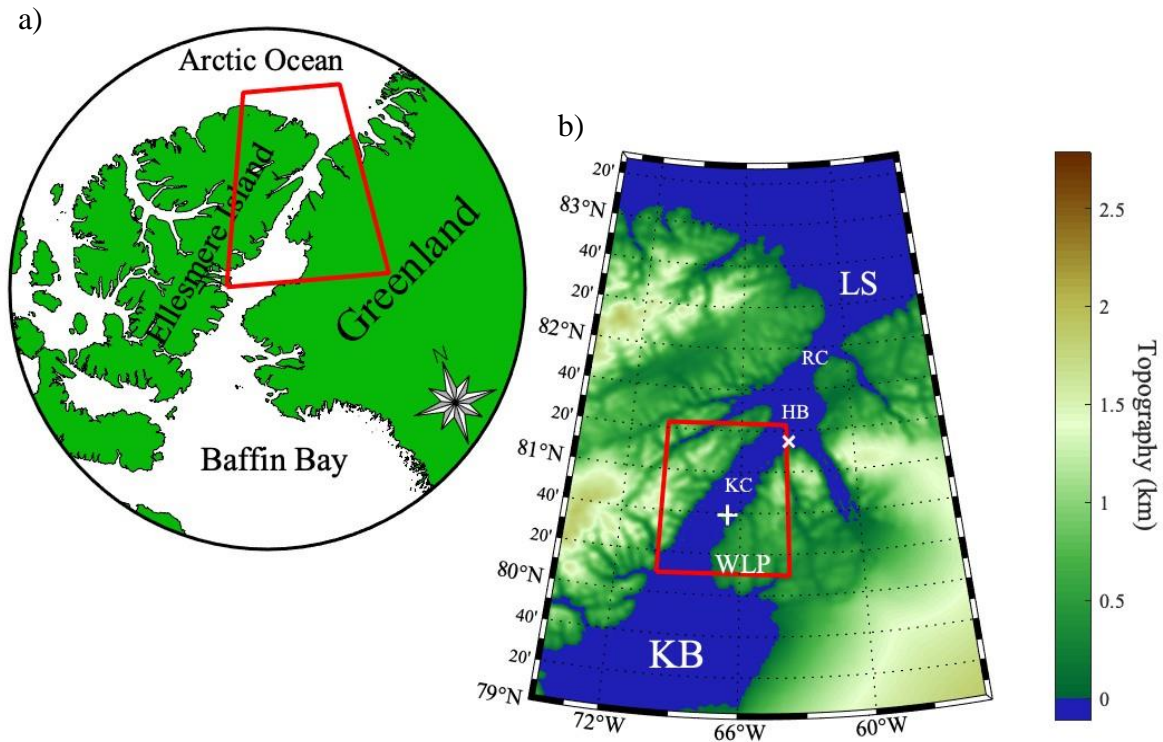
73   Richard et al., 1998).

a)

b)

Figure 1. Geographical maps showing a) the location of Nares Strait and b) an enlarged view of the red-boxed region showing the topography around northern Nares Strait with the red polygon showing the specific domain in which sea ice and winds were analyzed. The labelled locations near and on the strait are: the Lincoln Sea (LS), Robeson Channel (RC), Hall Basin (HB), Kennedy Channel (KC), Washington Land Peninsula (WLP), Kane Basin (KB), Joe Island (x), and Franklin Island (+).

74   In this study we identify previously unknown transient polynyas that develop along

75   Kennedy Channel that connects Hall Basin to Kane Basin (Fig. 1). These polynyas typically

76   form downwind of Joe Island and Franklin Island that are situated along the channel. The winds

77   along the channel tend to be enhanced as a result of its narrowness and the steep topography that

78   borders it (Moore & Imrit, 2022). We suggest a mechanism by which these islands shield

79   adjacent downwind areas from becoming ice-covered by southward sea ice flow as a result of

80   strong wind-forced advection.

81

82   **2 Materials and Methods**

83   **2.1 Datasets**

84   In order to investigate this phenomenon, sea ice concentration along Nares Strait was

85   retrieved with the ARTIST algorithm (Spreen et al., 2008) that makes use of data from the

86   Advanced Microwave Scanning Radiometers (AMSR-E and AMSR2). The ARTIST dataset has

87   a spatial resolution of approximately 3.125 km and is available from June 2002 – August 2023,

88   with a break between October 2011 and July 2012. In order to facilitate examination of

89   atmospheric conditions surrounding Nares Strait, 10 m wind speed, wind direction, and mean

90   sea-level pressure daily-averaged fields from the Copernicus Arctic Regional Reanalysis

91   (CARRA) were used (Schyberg et al., 2020). The CARRA fields are available at a resolution of

92   2.5 km for the period from September 1990 – May 2023.

93   Imaging/mapping of the sea ice along Nares Strait was achieved using AMSR sea ice

94   concentration data, MODIS (Moderate Resolution Imaging Spectroradiometer) infrared

95   channels, as well as the AMSR's 89 GHz brightness temperature channels. Upwards vertically

96   polarized emissions at 89 GHz made it possible to distinguish open water (greater brightness

97   temperature) from sea ice (lower brightness temperature).

98

99   **2.2 Choice of time period**

100   Nares Strait's mobile sea ice season typically lasts from mid/late summer to mid/late

101   winter (Vincent, 2019), with the rest of the year generally characterized by the presence of an ice

102   arch along the strait that inhibits sea ice flow. October was found to be the ideal month for our

103   analysis since it avoided the early sea ice transport season (September) during which sea ice

104   concentration is low, while also avoiding the early onset of the ice arch season, which can begin

105   as early as November. We did, however, redo our analysis for November and found similar

106   results.

107

108   **2.3 Peak Over Threshold Technique**

109   To quantify sea ice concentration variability within Kennedy Channel, a spatial domain

110   ranging from 80.16°N to 81.38°N latitude and 63.6°W to 70°W longitude was used (Fig. 1). The

111   mean daily ice concentration in this region was calculated for all October days on record. We

112   then employed a peak-over-threshold method by identifying the October dates with mean ice

113   concentration values that exceeded the 90th quantile value and the dates that lie below the 10th

114   quantile value, denoted as our high and low sea ice concentration events, respectively. In order

115   not to bias our results, instances of double counting whereby we identified several consecutive

116   days with a mean ice concentration that exceeded the thresholds were not considered. To account

117   for this, whenever multiple days were found to lie beyond the lower or upper thresholds, only the

118   dates with the lowest or highest values, respectively, within a 3-day period were considered in

119   the analysis. After identifying all dates that exceeded the thresholds, and accounting for the

120   described double counting, a total of 30 high sea ice event dates and 33 low sea ice event dates

121   were identified. We performed a repeat analysis by thresholding on extreme wind

122   speed/direction events as well and obtained similar results.

123   Following identification of the October dates that fit into either category, sea ice

124   concentration maps for northern Nares Strait for the high event dates and low event dates were

125   composited. For comparison, the sea ice concentration maps for all available October days were

126   also averaged to identify the climatological sea ice conditions. The 10 m wind vector fields and

127   sea-level pressure maps from CARRA data for the high and low sea ice event dates were also

128   composited and a climatological wind and sea-level pressure map was similarly obtained using

129   data from all available October days.

130   Daily latitudinal profiles of sea ice concentration and wind speeds along Nares Strait

131   were also constructed by determining median AMSR sea ice concentration and CARRA wind

132   speeds parallel to the strait along lines of constant latitude. Composites of high and low sea ice

133   event profiles were generated in order to facilitate a more quantitative treatment of our proposed

134   island phenomenon. The climatological latitudinal profile from all available October days from

135   2002 – 2022 was again determined for comparison. Furthermore, using a Monte Carlo approach,

136   the 1st quantile and 99th quantile of sea ice concentration and wind speed considering all October

137   days and at each available latitude were determined in order to characterize the statistical

138   significance of the high and low composites.

139   **3 Results**

140   **3.1 Temporal Variability of Sea Ice**

141   We calculated the mean daily sea ice concentration along Kennedy Channel during

142   October 2002 – 2022 and constructed a time series for a typical month — October 2022 (Fig. 2).

143   It is evident here that the sea ice concentration is quite variable with a mean of 64%, two events

144   where the ice concentration drops below the 10th quantile value of 53%, as well as two events

145   where the ice concentration rises above the 90th quantile value of 82%. Other Octobers during

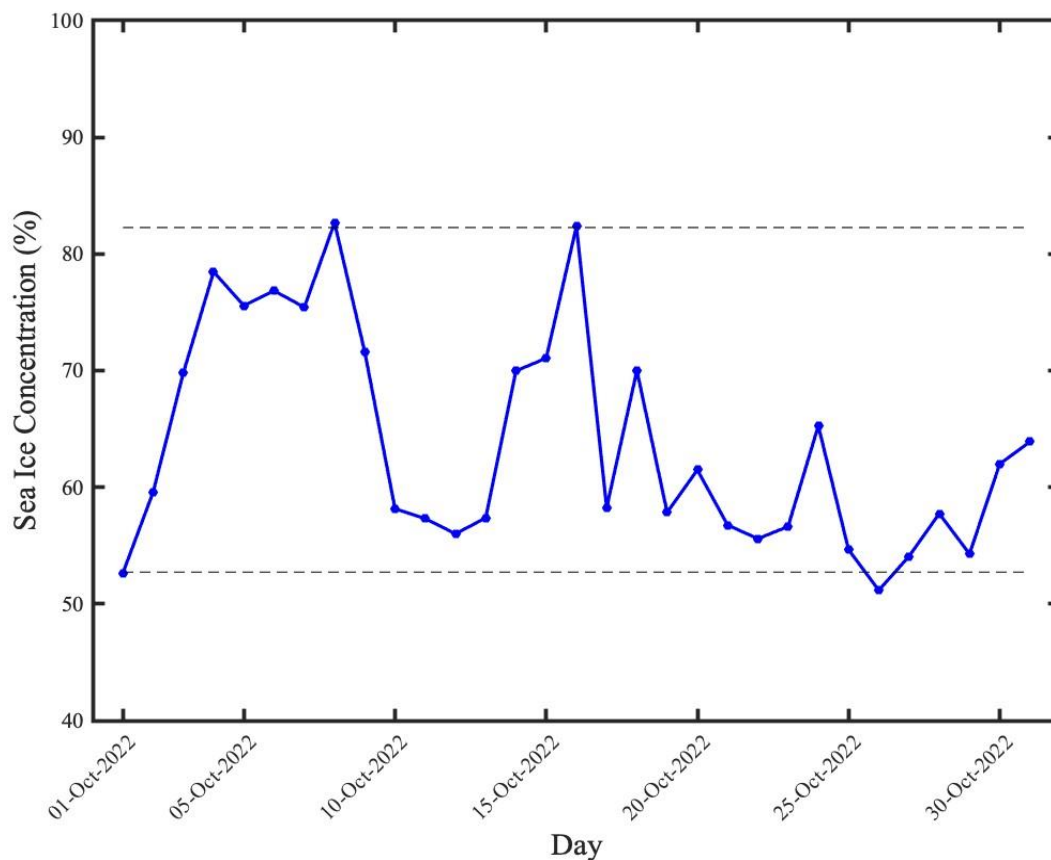146   the period of interest had similar distributions.

Figure 2. Time series of daily mean sea ice concentration (AMSR2) in Kennedy Channel during the
month of October 2022. The horizontal dashed lines show the 90th quantile (upper line) and 10th quantile
(lower line) values of mean daily sea ice concentration in this region during Octobers.

147   For the date that was identified with an average ice concentration lying below the lower

148   threshold — Oct 26, 2022 — the reduced ice cover was mapped/imaged (Fig. 3). In each image

149 high quantities of sea ice can be observed throughout the strait and Kennedy Channel, with

150 regions of open water and reduced ice cover southwards of Franklin Island and Joe Island.
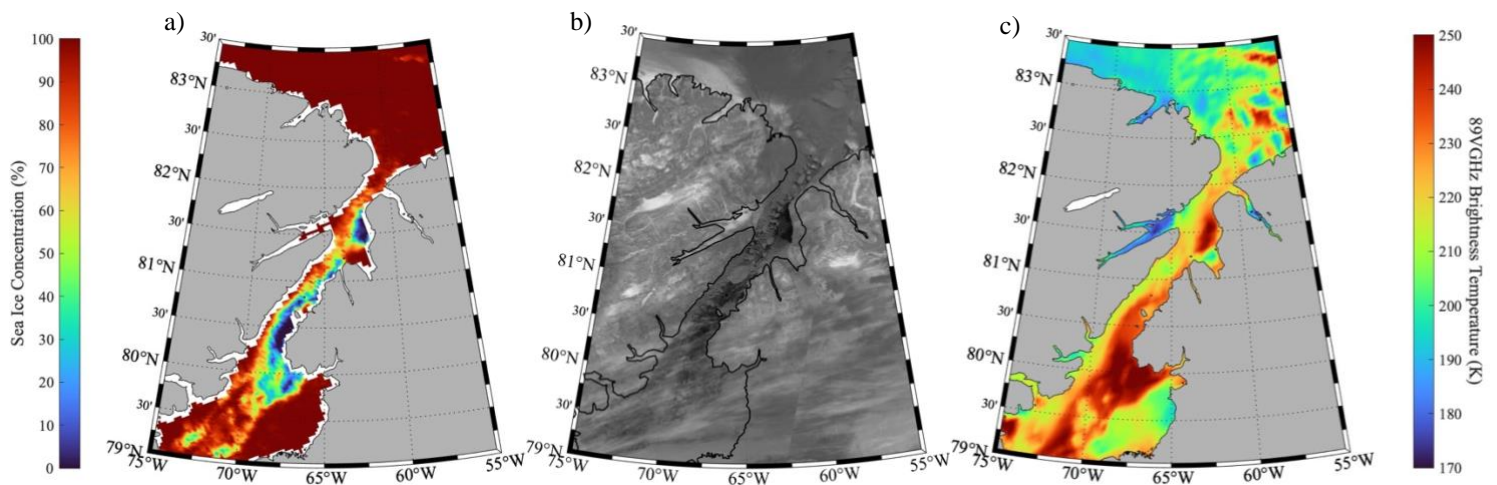

Figure 3. Kennedy Channel and Northern Nares Strait as viewed, using a) the mapping of AMSR2 sea ice concentration data, b) MODIS infrared imagery, and c) AMSR2 89GHz vertical polarization brightness temperature data, on October 26, 2022.

3.2 Spatial Variability of Sea Ice

151

152 The climatological sea ice distribution during October (Fig. 4a) indicates that the ice

153 concentration is close to 100% over the Lincoln Sea and decreases as one moves southwards

154 towards northern Kane Basin. Local minima occur south of Joe and Franklin Islands as well as

155 over northern Kane Basin south of the Washington Land Peninsula (Fig. 1). The low event

156 composite (Fig. 4b) has a quantitatively similar structure to the climatological case with

157 significantly reduced sea ice concentrations in the same locations. The high event composite

158 (Fig. 4c) shows nearly 100% ice cover from the Lincoln Sea down into Kane Basin, albeit with a

159 similar noticeable minimum south of the Washington Land Peninsula.

160 The median sea ice concentration along the strait as a function of latitude provides a more

161 quantitative view of sea ice variability in Nares Strait (Fig. 4d). Significant local minima for the

162 low event case are observed directly downstream of the latitudes of Joe and Franklin Islands.

163 Another local minimum is observed around 82°N. Interestingly, in the low composite, there was

164 a sharp increase in ice presence immediately north of Franklin Island prior to the subsequent

165 decrease to its south producing a sea ice dipole across the island. The climatological and high

166 event cases show less variability in median ice concentration and are characterized by weaker

167 local minima near the same latitudes as the low case. As expected, the lowest ice concentrations

168   occur for the low composite where, south of Joe Island, it approaches 45% and where, south of

169   Franklin Island, it reaches between 20% − 30%. The extrema in this low event case were also

170   found to lie outside of the range of extreme ice concentration variability of the climatological

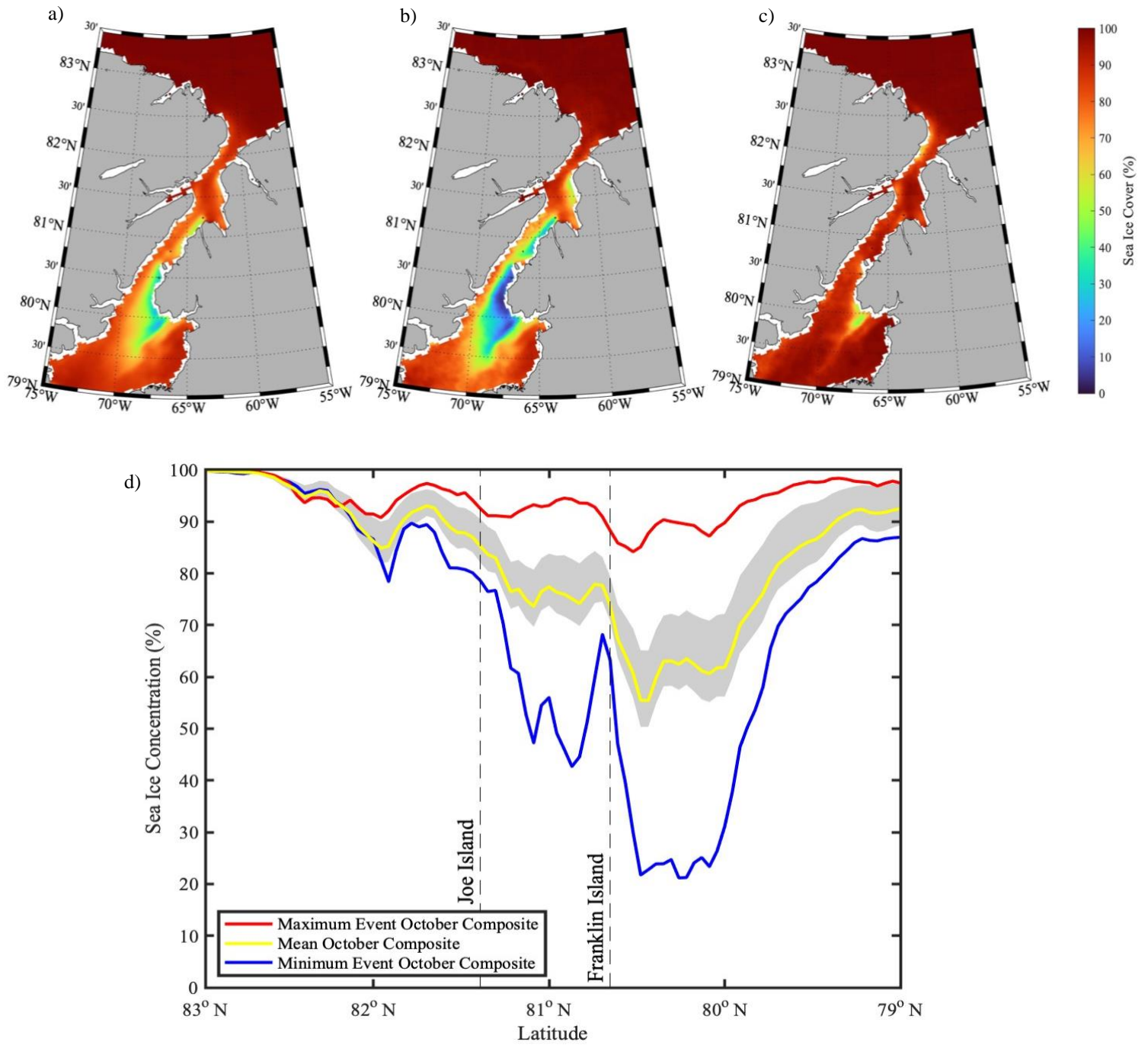171   October case represented by the shading.

172

173

Figure 4. October spatial sea ice concentration composites for northern Nares Strait from 2002 – 2022. The three images correspond to the averaging of a) all October days, b) only low event October days, and c) only high event October days. d) shows the median sea ice concentration by latitude along Nares Strait for each of the three sets of days. The shading represents the 1st and 99th quantile variability of sea ice concentration about the climatological composite at each latitude. The labeled dashed lines identify the latitudinal locations of Joe Island and Franklin Island.

174 **3.3 Spatial Variability of Wind and Mean Sea Level Pressure**

175   Composites of 10 m winds, 10 m windspeed, and sea level pressure for the low and high

176 events along with climatological conditions were produced in a similar fashion to the sea ice

177 maps (Fig. 5). The climatological October case (Fig. 5a) shows relatively weak winds in the

178 Lincoln Sea and Robeson Channel (Fig. 1), but stronger winds along Kennedy Channel and the

179 northwestern part of Kane Basin. The low event regime (Fig. 5b) shows significantly greater

180 wind speeds as compared to the climatological case, particularly within Kennedy Channel, and

181 has the strongest winds of the three composites. Furthermore, in these two cases the winds

182 generally lie parallel to the strait, with weaker winds in each of the composites occurring at sites

183 where the wind vectors are nearly parallel with the isobars (i.e. the Lincoln Sea, Hall Basin (Fig.

184 1), and southern Kane Basin). Conversely, the strongest winds, within Kennedy Channel, occur

185 where the wind vectors are nearly orthogonal on the isobars. The high event case (Fig. 5c) has

186 very weak winds throughout the strait. Interestingly, a wind reversal was present in this

187 composite which reached speeds of ~6 m/s in northern Robeson Channel and the Lincoln Sea.

188   The median wind speed parallel to the strait as a function of latitude (Fig. 5d) provides a

189 quantitative examination of the wind variability along the strait. Several local minima in winds

190 are located north of Joe Island in all three cases, as well as a broad minimum over Kennedy

191 Channel from just below 81.5°N to just above 80°N in the low and climatological cases. Again,

192 it is seen that the strongest wind speeds directed southwards along the strait occur for the low

193 event case reaching speeds of up to 12 m/s. Furthermore, this wind profile lies almost

194 consistently outside the extreme range of wind speed variability of the climatological October

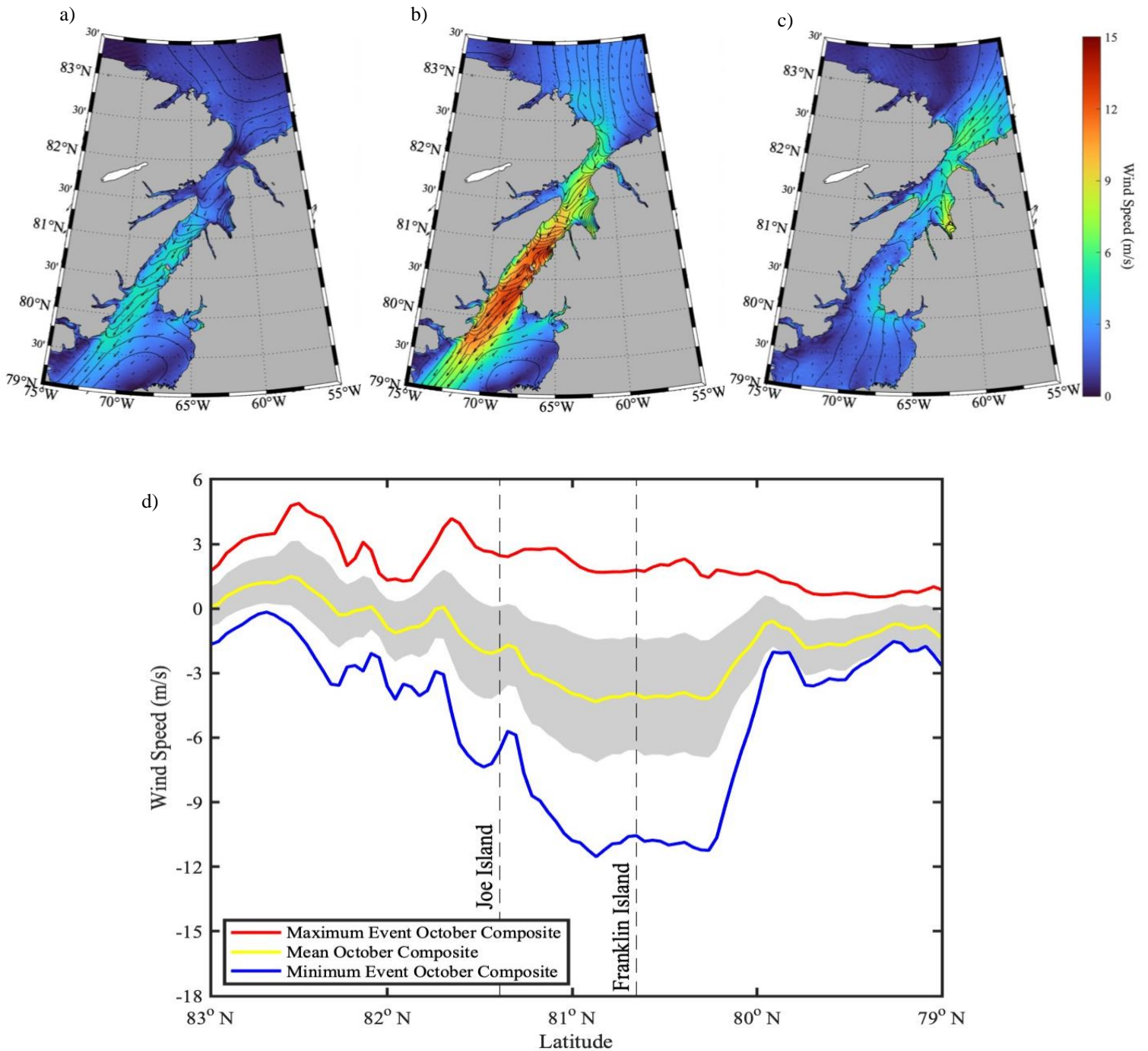195 case represented by the shading.

196

Figure 5. October spatial wind and pressure field composites for northern Nares Strait from 2002 – 2022. The maps show wind direction (vector field), wind speed (colourmap), and mean sea level pressure (isobar contours). The three composites were obtained from a) all October days, b) only low sea ice event days, and c) only high sea ice event days. d) shows the median wind speed parallel along the strait by latitude for each of the three sets of days. Positive values correspond to wind blowing up the strait while negative values correspond to wind blowing down the strait. The shading represents the 1st and 99th quantile variability of the wind speed about the climatological composite at each latitude. The labeled dashed lines identify the latitudinal locations of Joe Island and Franklin Island.

4 Discussion

In the low event case (Fig. 4b), it can be seen that the decrease in ice concentration within Kennedy Channel is the result of localized reductions at specific sites. The low ice concentrations south of the islands are believed to be caused by the advection of sea ice by winds into Kennedy Channel which, impinging upon the islands from the north, are diverted around them resulting in pockets of decreased concentration to form downwind. Since winds in this region generally blow from north to south (Moore, 2021), these polynyas tend to form off the southern faces of the islands.

These transient polynyas are believed to form analogously to wind-driven polynyas (Morales Maqueda et al., 2004) whereby coastal winds push sea ice away from land and expose open water. In Kennedy Channel, however, we propose that polynya production is caused by the southward wind-forced advection of ice around island obstacles, as opposed to the wind-forced removal of coastal ice.

Latitudinally, we find that the steepest local minima in ice concentration in the low event case occur south of the two islands, suggesting that it is indeed island effects that contribute to this behaviour (Fig. 4d). It is further seen that the minima latitudes in the low event October composite coincide with the minima in the climatological and high October composites at approximately 82°N and south of Joe and Franklin Islands' latitudes. This quantitively demonstrates that this ice-shielding effect is noticeable even during climatological, and to some extent during high October sea ice conditions.

With respect to the wind and sea level pressure results (Fig. 5), the flow along Kennedy Channel can be seen to be ageostrophic which, as discussed by Moore and Imrit (2022), is a consequence of the narrowness of the Strait. In the low event regime (Fig. 5b), the pressure gradient along Kennedy Channel is larger and thus there are correspondingly greater wind speeds as compared to climatological (Fig. 5a) and high event regimes (Fig. 5c). These enhanced winds contribute to a strong ice advection effect around the islands and induce the formation of larger polynyas (Fig. 4b). These results suggest that the strength of southward winds through Kennedy Channel are directly correlated to the size and amount of ice reduction within these polynyas. In the upper extreme case (Fig. 5c) there are relatively weak winds in Kennedy Channel, and correspondingly no polynya can be observed in the ice concentration composite (Fig. 4c). The

227 noticeable sea ice reduction south of the Washington Land Peninsula (Fig. 4c) does, however,

228 coincide with the ageostrophic flow of northwestern winds at this same site (Fig. 5c).

229   The wind fields in the low event composite and the climatological composite also reveal

230 the presence of a meso-scale region of low pressure situated towards the eastern edge of Kane

231 Basin bounded by the steep topography of the Washington Land peninsula to the north. This may

232 be an example of a lee cyclone (Buzzi et al., 2020). The associated cyclonic circulation is more

233 intense in the low event regime and would likely result in strong advection of sea ice away from

234 the south side of Washington Land Peninsula, therefore contributing to the sea ice reduction

235 observed here. It should be noted that a polynya had previously been identified in this region

236 during June by Kirillov et al. (2022), yet its production was attributed to the melting of ice

237 caused by the rising of warm subsurface water. We propose that a wind-driven sea ice advection

238 effect may work in tandem with the upwelling of warm water to contribute to the formation of

239 this polynya.

240   With respect to wind latitudinal profiles (Fig. 5d), the extreme winds in Kennedy channel

241 agree with spatial wind observations in the low event case (Fig. 5b). Comparison of the ice and

242 wind latitude profiles reveals that there is a correlated local minimum at approximately 82°N

243 shared among all composites. 82°N marks a transitionary site whereby the geostrophic flow from

244 the Lincoln Sea becomes ageostrophic in Robeson Channel (Fig. 5b). As the wind enters Nares

245 Strait from the north, the narrow channel and steep topography funnel and accelerate the winds,

246 thereby causing a spike in wind speed as observed in the wind speed profiles (Fig. 5d).

247 Coincident sea ice flow carried by these winds into the strait is likely also sped up leading to a

248 reduction and gap in ice presence as observed in the sea ice concentration profiles (Fig. 4d). This

249 effect, albeit a small one, still produces a noticeable impact even on the high sea ice composite

250 (Fig. 4d).

251   Downwind island effects have previously been shown to have far-reaching impacts on

252 wind and sea temperature patterns in the Pacific Ocean (Xie et al., 2001). There is also evidence

253 that the climatological easterly flow within the Chukchi Sea in the western Arctic Ocean results

254 in a latent heat polynya downstream of Wrangel Island (Moore & Pickart, 2012). Here we

255 identify previously unknown transient polynyas that form within the interior of Nares Strait due

256 to such downstream island effects. The presence of these open water regions likely also lead to

257 increased heat and moisture fluxes into the atmosphere from Kennedy Channel and potential

258 biological activity. Many Arctic species that overwinter in the Canadian Arctic Archipelago

259 (Pole, 2016) may use these polynyas and may rely on them in a future where the NOW does not

260 exist as it does today (Moore et al., 2023).

261

262 Acknowledgments

263

264 Open Research

265 AMSR-E and AMSR2 (Advanced Microwave Scanning Radiometer) data (Spreen et al., 2008)

266 are available at https://seaice.uni-bremen.de/sea-ice-concentration/amsre-amsr2/. AMSR2

267 brightness temperature data (Meier et al., 2018) is available at

268 https://nsidc.org/data/au_si6/versions/1#anchor-0. The CARRA (Copernicus Arctic Regional

269 Reanalysis) data (Schyberg et al., 2020) areavailable at

270 https://cds.climate.copernicus.eu/cdsapp#!/dataset/reanalysis-carra-single-levels?tab=overview.

References

Arrigo, K. R. (2007). Chapter 7 Physical Control of Primary Productivity in Arctic and Antarctic Polynyas. In W. O. Smith & D. G. Barber (Eds.), *Polynyas: Windows to the World* (Vol. 74, pp. 223–238). Elsevier. https://doi.org/https://doi.org/10.1016/S0422-9894(06)74007-7

Barber, D. G., Hanesiak, J. M., Chan, W., & Piwowar, J. (2001). Sea-ice and meteorological conditions in Northern Baffin Bay and the North Water polynya between 1979 and 1996. *Atmosphere - Ocean*, *39*(3), 343–359. https://doi.org/10.1080/07055900.2001.9649685

Barber, D. G., & Massom, R. A. (2007). Chapter 1 The Role of Sea Ice in Arctic and Antarctic Polynyas. In W. O. Smith & D. G. Barber (Eds.), *Polynyas: Windows to the World* (Vol. 74, pp. 1–54). Elsevier. https://doi.org/https://doi.org/10.1016/S0422-9894(06)74001-6

Buzzi, A., Davolio, S., & Fantini, M. (2020). Cyclogenesis in the lee of the Alps: a review of theories. *Bulletin of Atmospheric Science and Technology*, *1*(3), 433–457. https://doi.org/10.1007/s42865-020-00021-6

Finley, K. J., & Renaud, W. E. (1980). Marine Mammals Inhabiting the Baffin Bay North Water in Winter. *Arctic*, *33*(4), 724–738.

Heide-Jørgensen, M. P., Burt, L. M., Hansen, R. G., Nielsen, N. H., Rasmussen, M., Fossette, S., & Stern, H. (2013). The significance of the north water polynya to arctic top predators. *Ambio*, *42*(5), 596–610. https://doi.org/10.1007/s13280-012-0357-3

Heide-Jørgensen, M. P., Sinding, M.-H. S., Nielsen, N. H., Rosing-Asvid, A., & Hansen, R. G. (2016). Large numbers of marine mammals winter in the North Water polynya. *Polar Biology*, *39*(9), 1605–1614. https://doi.org/10.1007/s00300-015-1885-7

Howell, S. E. L., Babb, D. G., Landy, J. C., Moore, G. W. K., Montpetit, B., & Brady, M. (2023). A Comparison of Arctic Ocean Sea Ice Export Between Nares Strait and the Canadian Arctic Archipelago. *Journal of Geophysical Research: Oceans*, *128*(4). https://doi.org/10.1029/2023JC019687

Ingram, R. G., Bâcle, J., Barber, D. G., Gratton, Y., & Melling, H. (2002). An overview of physical processes in the North Water. *Deep-Sea Research Part II: Topical Studies in Oceanography*, *49*(22–23), 4893–4906. https://doi.org/10.1016/S0967-0645(02)00169-8

Kirillov, S., Dmitrenko, I., Babb, D. G., Ehn, J. K., Koldunov, N., Rysgaard, S., Jensen, D., & Barber, D. G. (2022). The role of oceanic heat flux in reducing thermodynamic ice growth

301   in Nares Strait and promoting earlier collapse of the ice bridge. *Ocean Science*, *18*(5),

302   1535–1557. https://doi.org/10.5194/os-18-1535-2022

303   Kottmeier, Ch., & Engelbart, D. (1992). Generation and atmospheric heat exchange of coastal

304   polynyas in the Weddell Sea. *Boundary-Layer Meteorology*, *60*(3), 207–234.

305   https://doi.org/10.1007/BF00119376

306   Marchese, C., Albouy, C., Tremblay, J. É., Dumont, D., D'Ortenzio, F., Vissault, S., & Bélanger,

307   S. (2017). Changes in phytoplankton bloom phenology over the North Water (NOW)

308   polynya: a response to changing environmental conditions. *Polar Biology*, *40*(9), 1721–

309   1737. https://doi.org/10.1007/s00300-017-2095-2

310   Meier, N., W., Comiso, J. C., & Markus, T. (2018). *AMSR-E/AMSR2 Unified L3 Daily 6.25 km*

311   *Polar Gridded 89 GHz Brightness Temperatures, Version 1* [Dataset]. NASA National

312   Snow and Ice Data Center Distributed Active Archive Center.

313   Møller, E. F., Johansen, K. L., Agersted, M. D., Rigét, F., Clausen, D. S., Larsen, J., Lyngs, P.,

314   Middelbo, A., & Mosbech, A. (2018). Zooplankton phenology may explain the North Water

315   polynya's importance as a breeding area for little auks. *Marine Ecology Progress Series*,

316   *605*, 207–223.

317   Moore, G. W. K. (2021). Impact of model resolution on the representation of the wind field

318   along Nares Strait. *Scientific Reports*, *11*(1), 1–14. https://doi.org/10.1038/s41598-021-

319   92813-9

320   Moore, G. W. K., Howell, S. E. L., & Brady, M. (2023). Evolving relationship of Nares Strait ice

321   arches on sea ice along the Strait and the North Water, the Arctic's most productive

322   polynya. *Scientific Reports*, *13*(1), 1–16. https://doi.org/10.1038/s41598-023-36179-0

323   Moore, G. W. K., & Imrit, A. A. (2022). Impact of Resolution on the Representation of the Mean

324   and Extreme Winds Along Nares Strait. *Journal of Geophysical Research: Atmospheres*,

325   *127*(19), 1–17. https://doi.org/10.1029/2022JD037443

326   Moore, G. W. K., & Pickart, R. S. (2012). The Wrangel Island Polynya in early summer: Trends

327   and relationships to other polynyas and the Beaufort Sea High. *Geophysical Research*

328   *Letters*, *39*(5), 1–5. https://doi.org/10.1029/2011GL050691

329   Morales Maqueda, M. A., Willmott, A. J., & Biggs, N. R. T. (2004). Polynya dynamics: A

330   review of observations and modeling. *Reviews of Geophysics*, *42*(1).

331   https://doi.org/10.1029/2002RG000116

332 Pole, N. (2016). *Canadian High Arctic-North Greenland LME*. 1–9.

333 Ribeiro, S., Limoges, A., Massé, G., Johansen, K. L., Colgan, W., Weckström, K., Jackson, R.,
334   Georgiadis, E., Mikkelsen, N., Kuijpers, A., Olsen, J., Olsen, S. M., Nissen, M., Andersen,
335   T. J., Strunk, A., Wetterich, S., Syväranta, J., Henderson, A. C. G., Mackay, H., …
336   Davidson, T. A. (2021). Vulnerability of the North Water ecosystem to climate change.
337   *Nature Communications*, *12*(1). https://doi.org/10.1038/s41467-021-24742-0

338 Richard, P. R., Orr, J. R., Dietz, R., & Dueck, L. (1998). Sightings of Belugas and Other Marine
339   Mammals in the North Water, Late March 1993. *Arctic*, *51*(1), 1–4.

340 Schyberg, H., Yang, X., Køltzow, M. A. Ø., Amstrup, B., Bakketun, Å., Bazile, E., Bojarova, J.,
341   Box, J. E., Dahlgren, P., Hagelin, S., Homleid, M., Horányi, A., Høyer, J., Johansson, Å.,
342   Killie, M. A., Körnich, H., Le Moigne, P., Lindskog, M., Manninen, T., … Wang, Z. Q.
343   (2020). *Arctic regional reanalysis on single levels from 1991 to present*. Copernicus
344   Climate Change Service (C3S) Climate Data Store (CDS).
345   https://doi.org/10.24381/cds.713858f6

346 Smedsrud, L. H., Halvorsen, M. H., Stroeve, J. C., Zhang, R., & Kloster, K. (2017). Fram Strait
347   sea ice export variability and September Arctic\hack{\newline} sea ice extent over the last
348   80 years. *The Cryosphere*, *11*(1), 65–79. https://doi.org/10.5194/tc-11-65-2017

349 Smith, S. D., Muench, R. D., & Pease, C. H. (1990). Polynyas and leads: An overview of
350   physical processes and environment. *Journal of Geophysical Research: Oceans*, *95*(C6),
351   9461–9479. https://doi.org/https://doi.org/10.1029/JC095iC06p09461

352 Spreen, G., Kaleschke, L., & Heygster, G. (2008). Sea ice remote sensing using AMSR-E 89-
353   GHz channels. *Journal of Geophysical Research: Oceans*, *113*(2), 1–14.
354   https://doi.org/10.1029/2005JC003384

355 Steffen, K. (1985). Warm water cells in the North Water, Northern Baffin Bay during winter.
356   *Journal of Geophysical Research: Oceans*, *90*(C5), 9129–9136.
357   https://doi.org/10.1029/jc090ic05p09129

358 Tremblay, J.-E., & Smith, W. O. (2007). Chapter 8 Primary Production and Nutrient Dynamics
359   in Polynyas. In W. O. Smith & D. G. Barber (Eds.), *Polynyas: Windows to the World* (Vol.
360   74, pp. 239–269). Elsevier. https://doi.org/https://doi.org/10.1016/S0422-9894(06)74008-9

361 Vincent, R. F. (2019). A Study of the North Water Polynya Ice Arch using Four Decades of
362   Satellite Data. *Scientific Reports*, *9*(1), 20278. https://doi.org/10.1038/s41598-019-56780-6

363   Weingartner, T. J., Cavalieri, D. J., Aagaard, K., & Sasaki, Y. (1998). Circulation, dense water

364   formation, and outflow on the northeast Chukchi Shelf. *Journal of Geophysical Research:*

365   *Oceans*, *103*(C4), 7647–7661. https://doi.org/https://doi.org/10.1029/98JC00374

366   Xie, S. P., Liu, W. T., Liu, Q., & Nonaka, M. (2001). Far-Reaching effects of the Hawaiian

367   islands on the Pacific Ocean-Atmosphere system. *Science*, *292*(5524), 2057–2060.

368   https://doi.org/10.1126/science.1059781

369